ADVANCED FUNCTIONAL MATERIALS
www.afm-journal.de

Chiral Plasmonic Response of 2D $Ti_3C_2T_x$ Flakes: Realization and Applications

*A. Olshtrem, I. Panov, S. Chertopalov, K. Zaruba, B. Vokata, P. Sajdl, J. Lancok, J. Storch, V. Církva, V. Svorcik, M. Kartau, A. S. Karimullah, J. Vana, and O. Lyutakov**

The circularly polarized light sensitive materials response can be reached at plasmon wavelengths through the coupling of intrinsically non-chiral plasmonic nanostructure with chiral organic molecules. As a plasmonic background, the different types of metal nanoparticles of various shapes and sizes are successfully tested and an apparent circular dichroism (CD) signal is measured in both, nanoparticles suspensions and after nanoparticle immobilization in substrate. In this work, the creation of plasmon-active 2D flakes of MXenes ($Ti_3C_2T_x$) is proposed, with the apparent CD response at plasmon wavelength, through the coupling of intrinsically non-chiral flakes with helically shaped helicene enantiomers. This work provides the first demonstration of chiral and plasmon-active 2D material, which shows the absorption sensitive to light intrinsic circular polarization even in plasmon wavelengths range. The appearance of the induced CD signal is additionally confirmed by several theoretical calculations. After the experimental and theoretical confirmation of the optical chirality at plasmon wavelengths, the flakes are utilized for the polarization sensitive conversion of light to heat, as well as for polarization dependent triggering of plasmon-assisted chemical transformation.

1. Introduction

Chirality as a basic feature of nature occurs as a basic property from molecular up to global galactic levels.[1,2] Recently significant efforts have been directed to the creation and utilization of artificial chiral nanostructures.[3,4] Among them the chiral plasmonic structures deserve special attention, since they can ensure polarization-sensitive manipulation with light at a sub-diffraction level.[5–7] A great number of chiral plasmonic structures were proposed recently and their utilization in the fields of enantioselective detection as well as chiral catalysis has been successfully demonstrated.[8]

Common routes for chiral plasmonic nanostructures creation involve the 2D or 3D lithographic approaches, metal nanoparticles self-assembling as well as chirality introduction at the level of the nanoparticles morphology.[9–12] As an alternative, the metal sputtering on specially etched surfaces, shadow metal(s) deposition or patterned metal surfaces twisting can be mentioned.[13–15] The creation of well-defined nanostructures often requires complex processes, while utilization of simpler techniques often do not show a satisfactory value of polarization-dependent light absorption.[9,10,13–15] As an interesting alternative, the simple but efficient approach for realization of chirality at plasmon wavelength through the coupling of intrinsically non-chiral plasmonic nanoparticles with chiral (dielectric) molecules

A. Olshtrem, V. Svorcik, O. Lyutakov
Department of Solid State Engineering
University of Chemistry and Technology
16628 Prague, Czech Republic
E-mail: lyutakoo@vscht.cz

I. Panov, V. Církva
Group of Advanced Materials and Organic Synthesis
Institute of Chemical Process Fundamentals
Czech Academy of Sciences
165 02 Prague, Czech Republic

S. Chertopalov, J. Lancok, J. Storch
Institute of Physics of the Czech Academy of Sciences
18221 Prague, Czech Republic

The ORCID identification number(s) for the author(s) of this article can be found under https://doi.org/10.1002/adfm.202212786.

DOI: 10.1002/adfm.202212786

K. Zaruba
Department of Analytical Chemistry
University of Chemistry and Technology
16628 Prague, Czech Republic

B. Vokata
Department of Biochemistry and Microbiology
University of Chemistry and Technology
16628 Prague, Czech Republic

P. Sajdl
Department of Power Engineering
University of Chemistry and Technology
16628 Prague, Czech Republic

M. Kartau, A. S. Karimullah
School of Chemistry
Joseph Black Building
University of Glasgow
Glasgow G12 8QQ, UK

J. Vana
Institute of Organic Chemistry and Technology
Faculty of Chemical Technology
University of Pardubice
53210 Pardubice, Czech Republic

was proposed.[16–23] In this case, chirality arises from the dipole–dipole (or multipole) based interaction of plasmonic nanostructures with chiral environment and chirality appearance was demonstrated for various shapes of a metal nanostructures, including spherical AuNPs, Au nanorods, and silver nanocubes, as well as dimers or multimers of different nanoparticles.[17–19,22–32] In addition to plasmon-active metal nanoparticles, the explicit polarization-dependent interaction of larger (non-plasmonic and non-chiral) nanoparticles with circularly polarized light was described in[33,34] as a function of their chiral environment.

Beyond the well-studied plasmon-active metal nanoparticles or patterned metal surfaces, a recently discovered class of 2D materials—so-called MXene—also shows an apparent plasmon absorption at visible wavelengths.[35–37] In this work, we have demonstrated for the first time the ability to induce a chiral response of MXene ($Ti_3C_2T_x$) flakes at plasmon wavelengths by their coupling with highly chiral helicene enantiomers (samples are further designated as $Ti_3C_2T_x$-Hel). Such an approach allows us to reach the polarization sensitive response of 2D flakes, which is based on dielectric environment induced chirality transfer. This is quite different from the previously reported case, where the chirality was reached through specific flakes shape and/or atoms arrangement.[38] We also demonstrated several potential applications of created chiral 2D materials, combining together the more attractive areas of chiral plasmonic nanostructures and MXenes utilization[39–54] with main focus on polarization (circular)-sensitive applications.

2. Results and Discussion

2.1. Main Experimental Concept

Our main experimental concept is schematically represented in **Figure 1**. We used the $Ti_3C_2T_x$ flakes prepared by conventional etching and delamination of the corresponding MAX phase (see Supporting Information for details). In parallel, the enantiopure helicenes with $-NH_2$ substituent were prepared. The helicene enantiomers exhibit unique chiroptical properties and huge values of optical rotation, e.g., specific optical rotations for unsubstituted (P)- and (M)-[6]helicene were found to be $2935 \pm 4°$ and $-2883 \pm 2°$ respectively. To place $Ti_3C_2T_x$ flakes and helicene enantiomers in close proximity and create covalent bond between them, we diazotized the amino groups in helicene structure and grafted the helicene enantiomers onto flakes surface either through the formation of a direct Ti—Hel bonds or through oxygen bridges due to the interaction of diazohelicenes with the =O or —OH MXene terminated groups. After enantiomers grafting one can expect that chirality will appear at flakes plasmon wavelengths due to the dipole–dipole (or multipole) interactions between plasmon active $Ti_3C_2T_x$ flakes and closed helical enantiomers, as was theoretically predicted and experimentally confirmed earlier.[17–19,24–28] In the final step we tested the created materials for polarization-sensitive application in light to heat conversion and plasmon-assisted chemical transformation.

2.2. Optimization and Confirmation of Helicene Enantiomers Grafting

To optimize the grafting time, we performed a series of time-resolved UV–vis and Raman measurements (more precisely, Surface Enhanced Raman Spectroscopy (SERS) measurements, since 785 nm excitation wavelength was used). For clarity we present only the results obtained with (P)-Hel enantiomer, but there was no fundamental difference between the (P)- and (M)-Hel enantiomers. Absorption spectra, measured after (P)-Hel grafting reveal a shift in the position of $Ti_3C_2T_x$ plasmon absorption band due to changes in dielectric constants of flakes closed environment (**Figure 2**A). More importantly, the characteristic for helicene absorption band (Figure S1, Supporting Information) appears at near-UV wavelengths and its intensity

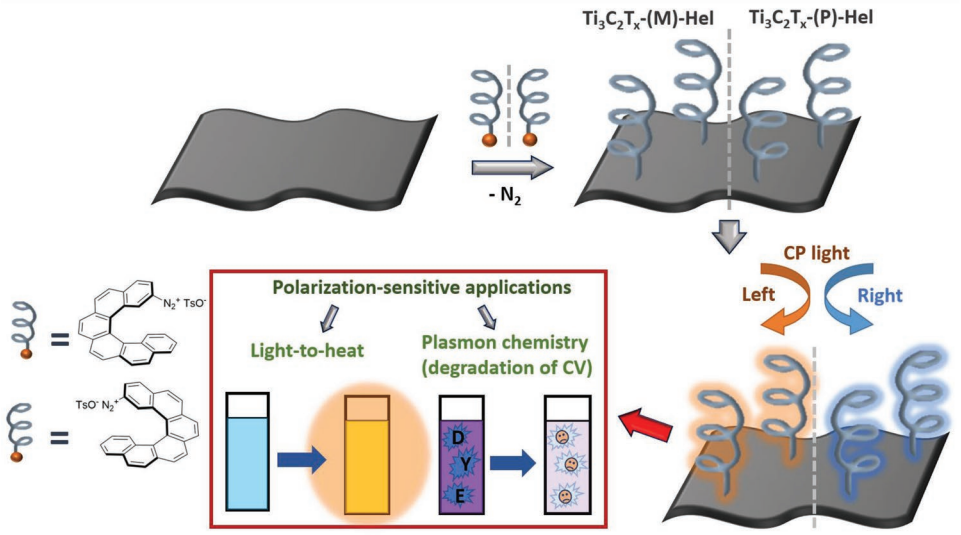

Figure 1. Schematic representation of proposed experimental concept: grafting of $Ti_3C_2T_x$ with enantiopure helicenes using the diazonium chemistry approach for realization of chiral 2D materials.

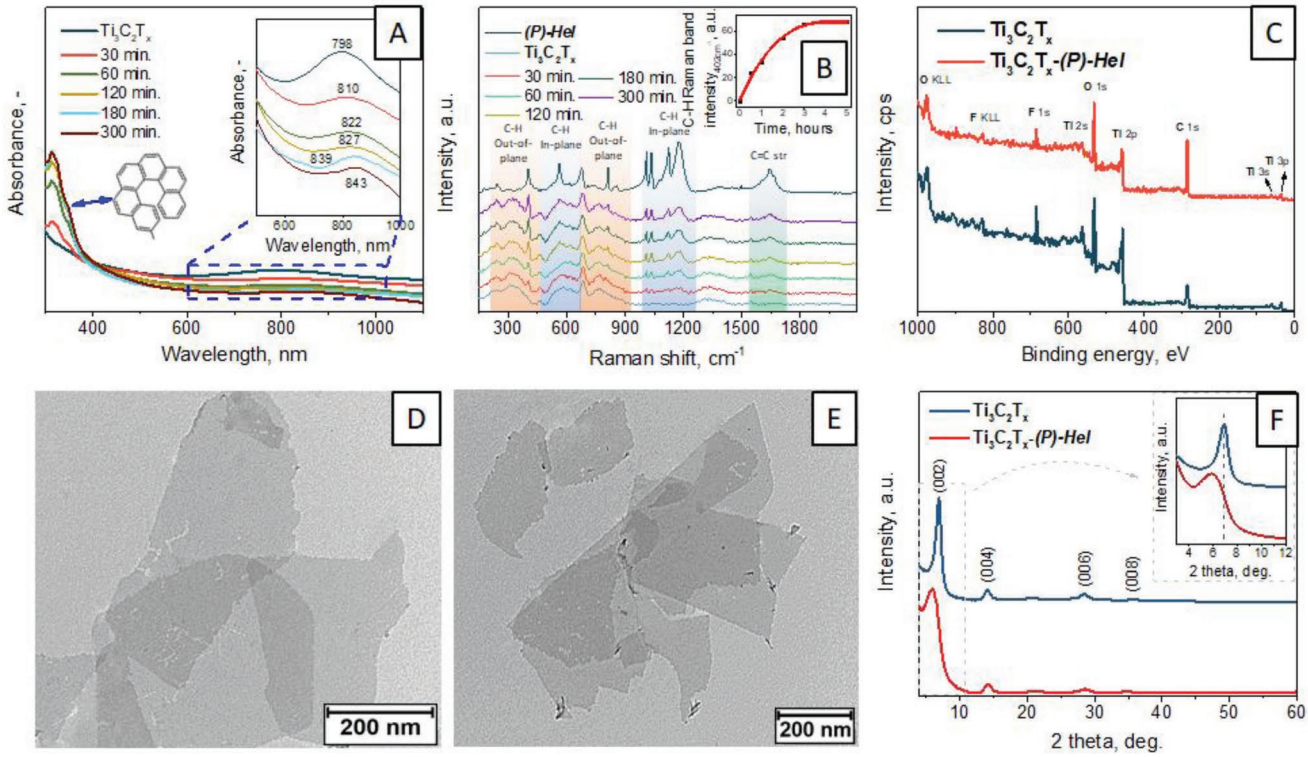

Figure 2. $Ti_3C_2T_x$-Hel flakes characterization: A) UV–Vis spectra, measured after different time of $Ti_3C_2T_x$ coupling with (P)-Hel; B) SERS spectra of pristine $Ti_3C_2T_x$ flakes and (P)-Hel, SERS spectra of $Ti_3C_2T_x$-(P)-Hel flakes; C) XPS survey spectra of $Ti_3C_2T_x$ and $Ti_3C_2T_x$-(P)-Hel flakes D,E) TEM images of $Ti_3C_2T_x$ and $Ti_3C_2T_x$-(P)-Hel flakes; F) XRD patterns of $Ti_3C_2T_x$ and $Ti_3C_2T_x$-(P)-Hel flakes.

gradually increases with prolongation of the grafting time during the first 3 h of grafting. The surface attachment of helicene also resulted in the appearance of several characteristic SERS bands, attributed to the helicene structure (Figure 2B; Table S1, Supporting Information). As in the previous case, the prolongation of the grafting time leads to a gradual increase in helicene bands intensities which reaches a saturation after 3 h of grafting (Figure 2B, insert). So, it can be concluded that the coupling (grafting) of helicene molecules and flakes really proceeds and the $Ti_3C_2T_x$ surface is completely saturated by attached moieties after a certain time. This grafting time (3 h) is therefore used in all further experiments.

The flakes modification was additionally confirmed by X-ray photoelectron spectroscopy (XPS). The XPS survey spectra (Figure 2C; Figure S2, Supporting Information) show an increase of surface carbon concentration and decrease of Ti, O, and F characteristic peaks intensities due to screening by "large" helicenes molecules. The attenuation of Ti (2s) characteristic peak allows us to estimate the "average" thickness of grafted organic layer, which was found to be slightly above 1 nm, i.e., indicating the formation of relatively closed-packed helicene "monolayer" on flakes surface (see Supporting Information for details). The SERS spectra (Figure 2B) also show the preservation of the $Ti_3C_2T_x$ flakes characteristic features (wide bands, located in 150–550, 600–900, and 1200–1500 cm^{-1} spectral regions) that indirectly indicate the preservation of flakes crystallinity and 2D structure. The $Ti_3C_2T_x$ flakes survival was additionally confirmed by X-ray diffraction (XRD) and transmission electron microscopy (TEM) techniques. Results of TEM reveal the conservation of flakes geometry and size after the grafting (Figure. 2D,E, Figure S3, Supporting Information). In turn, the XRD pattern of $Ti_3C_2T_x$-Hel (Figure 2F) remains almost unchanged, compared to pristine $Ti_3C_2T_x$ flakes case. Just slight shift of reflexes to low angles was observed on XRD patterns (Figure 2F) after helicene grafting, which can be attributed to tuning of interlayer distance in flake(s) structure due to changes of flakes surface termination and expulsion of water molecules from interlayer space.

2.3. Optical Chirality and CD Response of $Ti_3C_2T_x$-Hel Flakes

In the next step, we proceed to the estimation of chirality appearance at characteristic $Ti_3C_2T_x$ plasmon wavelengths. As is evident from UV–vis spectra (Figure 2A) $Ti_3C_2T_x$ flakes have apparent plasmon related absorption band, located near 800 nm, which is red-shifted after the helicenes grafting. The helicene enantiomers are transparent at this and close wavelengths, but they have an apparent absorption band below 400 nm (Figure S1, Supporting Information) with corresponding pronounced CD signal at these wavelengths (**Figure 3**A). CD measurements of pristine $Ti_3C_2T_x$ flakes showed absence of CD signal in all optical ranges, including the range of plasmon resonance (Figure 3B,C). However, the CD spectra of $Ti_3C_2T_x$-(P)-Hel and $Ti_3C_2T_x$-(M)-Hel flakes, exhibit two spectral ranges with non-zero CD signal. The first one below 400 nm, attributed to the presence of helicene enantiomers could be expected. However, the second CD band(s) are located at the plasmon

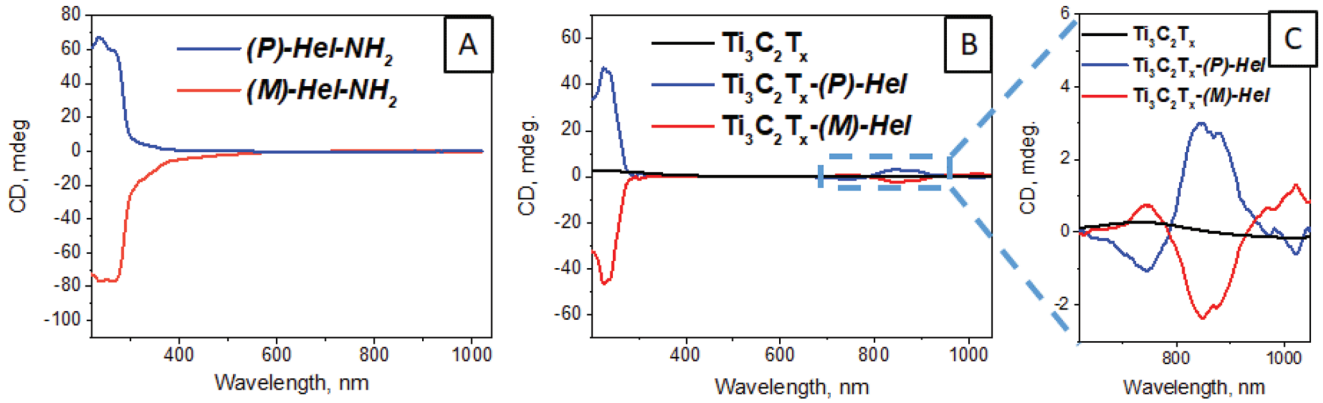

Figure 3. CD spectra of: A) - (P) and (M) helicene enantiomers (with the amino-group at position 2); B,C) - pristine $Ti_3C_2T_x$, $Ti_3C_2T_x$-(P)-Hel, and $Ti_3C_2T_x$-(M)-Hel flakes.

absorption wavelengths, i.e., near 800 nm. In this case the sign of CD signal, measured on $Ti_3C_2T_x$-(P)-Hel and $Ti_3C_2T_x$-(M)-Hel flakes is determined by the grafted helicene enantiomers (i.e., (P)-Hel or (M)-Hel) and it is in coincidence with them. So, our initial assumption is right grafting of helicenes to plasmon active flakes allows to reach the optical chirality at plasmon wavelengths in 2D material (similarly to previously reported case of plasmon-active nanoparticles with different shapes[17–19,24–28]). To our knowledge, this is a first observation of circular polarization sensitive light absorption at plasmon wavelengths within a flake's suspension, i.e., in the form of separated, individual (and probably single) flake(s).

As was mentioned above, the CD signal at plasmon wavelengths can be induced by coupling of intrinsically non-chiral plasmonic nanoparticles with surrounding monolayer of chiral molecules. From the theoretical point of view, this phenomenon can be due to the chiral charge distribution that alters the plasmonic resonance of the nanoparticles by a near-field dipole–dipole (or multipole) coupling.[20,30,55] To explain the observed chirality appearance, we also performed several simulations, based on the optical parameters of $Ti_3C_2T_x$ (extracted from AdR1) and optical parameters of helicenes determined separately (Figure S4, Supporting Information). Numerical calculations were performed using the wave optics module (COMSOL) for simulation of the electromagnetic fields produced across helicene and MXenes. Periodic boundary conditions were applied and perfectly matched layer conditions were applied to both input and output ports to minimize internal reflections. Obtained results are presented in Figure S5 (see Supporting Information for more experimental details) and clearly indicate that helicene enantiomers "grafting" induced chirality at MXene-related plasmon wavelengths. Without a doubt, these results are very tentative (although they provide a solid theoretical justification for the observed chirality transfer) and will be improved in the future.

We also observed some decrease in the intensity of the CD signal in the characteristic spectral region of the helicenes response (Figure 3). This fact can be explained by the different concentrations of helicenes in the initial solution and in the suspension of $Ti_3C_2T_x$-Hel flakes (since not all helicene molecules are grafted). Of course, in this case, it is impossible to conclude whether the CD signal of helicenes is enhanced or reduced after their grafting to the surface of plasmon-active 2D material.

2.4. Polarization-Sensitive Utilization of $Ti_3C_2T_x$-Hel Flakes

After the confirmation of $Ti_3C_2T_x$-Hel flakes plasmonic chirality we proceed to utilization of the created 2D material in two applications, where the absorption sensitive to circularly polarized light and unique properties of MXenes can play a crucial role. In particular, application of created material in polarization-sensitive plasmon-assisted photo-catalysis and polarization-sensitive light to heat conversion were studied. The latter one started from the assumption that $Ti_3C_2T_x$ flakes have excellent light to heat conversion efficiency,[54,56] while the presence of grafted helicenes can provide different absorption of left circular-polarized (LCP) and right circular-polarized (RCP) lights. For experimental evidence of so-called of photothermal chirality,[45] we illuminated the $Ti_3C_2T_x$-(P)-Hel and $Ti_3C_2T_x$-(M)-Hel flakes suspensions with LCP, RCP and non-circularly polarized (NP) laser light (850 nm) and measured the overall increase of suspension temperature (**Figure 4**A,B) and local temperature increase in the laser beam spot on suspension (Figure 4C,D). In the first case (Figure 4A,B), we observed an increase in local or general temperature, which reached a plateau after 40 min. In general, the results obtained clearly indicate that both, local and overall suspension temperatures depend on light and material chirality. In particular we observed the difference closed to 3 °C in overall temperature between illuminations of $Ti_3C_2T_x$-(P)-Hel suspension with RCP versus LCP or NP light (Figure 4A). Illumination of $Ti_3C_2T_x$-(M)-Hel flakes suspension led to symmetrically opposite results the suspension was heated more when using LCP light (Figure 4B). At this stage, it is worth noting that the observed values of the temperature difference exceeded the theoretically calculated ones (based on the CD spectra, details are given in Supporting Information). This discrepancy can be explained by an increased concentration of MXene flakes in the suspension used for polarization-dependent light-to-heat conversion, which can lead to flakes stacking and an increase in CD signal (which, in turn, is confirmed by above mentioned calculations performed for "thicker" MXene-Hel structures – Figure S5 Supporting Information). To verify the light polarization impact on light to heat

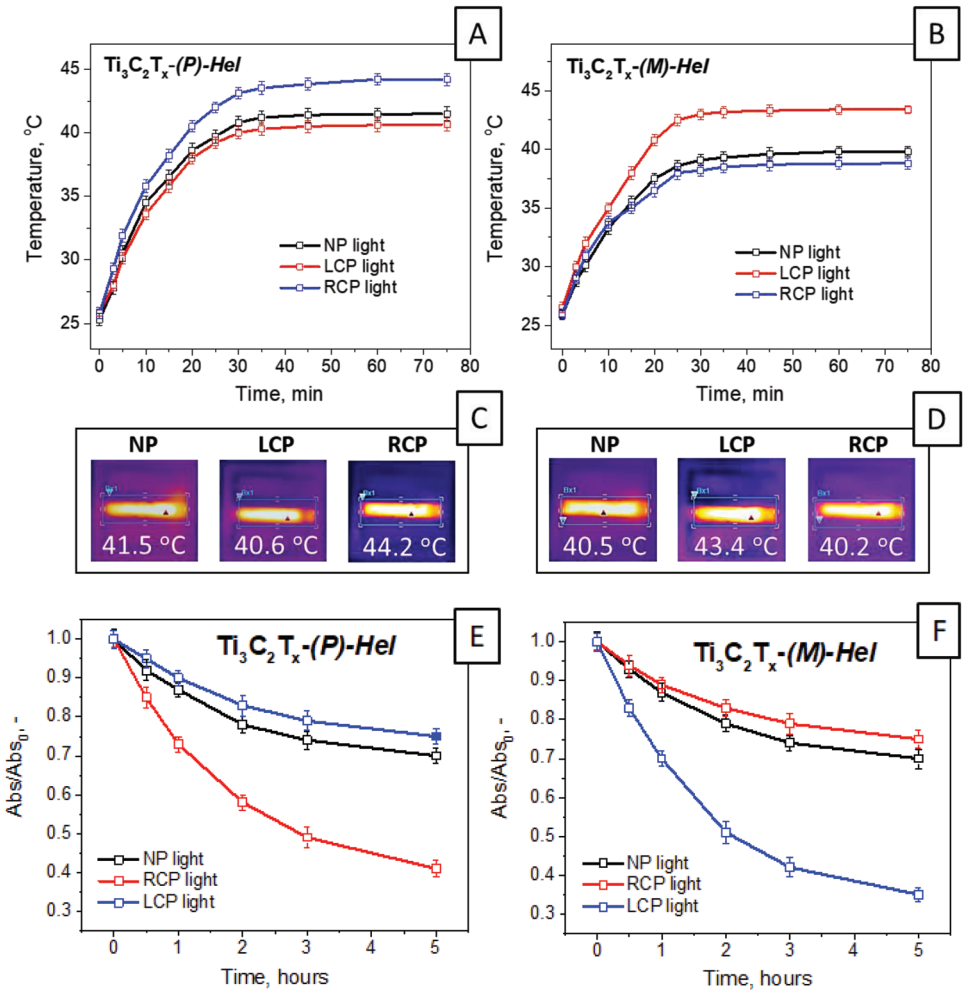

Figure 4. Demonstration of potential chiral 2D flakes utilization: A,B) Plasmon-induced heating of $Ti_3C_2T_x$-(P)-Hel and $Ti_3C_2T_x$-(M)-Hel flakes suspensions as a function of light (850 nm) polarization; C,D) Local heating (photos from thermocamera) of $Ti_3C_2T_x$-(P)-Hel and $Ti_3C_2T_x$-(M)-Hel flakes suspensions under passing of not-polarized of circularly polarized laser beam; E,F) Plasmon-induced degradation of CV dye as a function of laser light polarization (850 nm).

conversion definitively pristine $Ti_3C_2T_x$ flakes were illuminated with LCP, RCP, and NP light in a control experiment (Figure S6, Supporting Information) and no changes in temperature with light circular polarization switching were observed. It should be also noted that the observed difference in local temperature (for $Ti_3C_2T_x$-(P)-Hel and $Ti_3C_2T_x$-(M)-Hel flakes) increase was also apparent, which is evident from Figure 4C,D. These results show that in addition to the previously proposed utilization of the photothermal response of chiral nanomaterials in thermal energy conversion and electronic applications,[45] the $Ti_3C_2T_x$-Hel flakes with local, polarization sensitive heating can also potentially be used in advanced photothermal therapy (also taking into account the "bio-reasonable" heating, corresponding to the commonly reported one for this application[57,58]), under improved temperature control.

We also compared our results with previously published results for enantioselective light absorption.[45,59] As a plasmon-active source of chirality, the authors of[45,59] used the so-called gold helicoids, with not only higher CD signal index but also higher absorption coefficient (including light scattering), which cannot be neglected in the case of nanoparticles with a size close to 100 nm. It should be noted that the temperature difference observed in this study is much higher than those expected from previously published works[45,59] based on gold nanostructures. The observed temperature difference may be due to two factors, the significantly higher efficiency of $Ti_3C_2T_x$ material for light-temperature conversion (attributed to enhanced light-matter interaction and internal reflexions between the layers) and the related light-to-heat conversion efficiency close to 100%.[60–62] To test this hypothesis, we performed another comparative experiment using gold nanorods, which also show a plasmon absorption band near 800 nm and are known for their relatively good light-to-heat conversion efficiency and $Ti_3C_2T_x$ flakes (Figure S7, Supporting Information). Although we used solutions with the same extinction coefficient (at 780 nm), the $Ti_3C_2T_x$ suspension heated up much faster. Thus, the observed temperature difference can be related to both the absorption difference between left and right rotating light and the enhanced light-matter interaction (and related unique light-to-heat efficiency conversion) in the case of $Ti_3C_2T_x$ flakes.

Finally, we also demonstrated the potential of $Ti_3C_2T_x$-Hel flakes in polarization-sensitive, plasmon assisted photochemistry. This field could be considered as a hot topic, but it should be noted, that the most recent works were focused on the utilization of enantio-selective molecules sorption near plasmonic surface before plasmon-assisted reaction proceeding.[63,64] In our case we chose an alternative approach, with utilization of RCP or LCP light illumination for polarization-sensitive triggering of chemical transformation. As a model reaction we chose the plasmon-assisted degradation of dye (crystal violet (CV)), since this reaction was widely reported in the literature[65–67] and reaction efficiency can be simply estimated using the UV–Vis measurements (Figure S8, Supporting Information). Before plasmon-assisted triggering of CV degradation we performed several control experiments. Illumination of CV solution without addition of $Ti_3C_2T_x$ flakes does not lead to dye concentration decrease (Figure S9A, Supporting Information), which could be expected, since CV does not absorb the used light emitting diode (LED) wavelength. Slight decrease of CV solution absorption was observed after the simple interaction with $Ti_3C_2T_x$ flakes in dark since this cationic dye is probably entrapped by negatively charged flakes surface (Figure S9B, Supporting Information). On the other hand, dye entrapping was partially quenched after the flakes grafting with helicenes enantiomers. In turn, illumination of CV solution mixed with $Ti_3C_2T_x$ flakes suspension led to apparent decrease of CV concentration, indicating the plasmon-assisted dye degradation, which proceeds independently on the light polarization in the case of pristine $Ti_3C_2T_x$ flakes (Figure S10, Supporting Information). The impact of light polarization on the kinetic of dye degradation mediated by $Ti_3C_2T_x$-(P)-Hel and $Ti_3C_2T_x$-(M)-Hel flakes can be seen from Figure 4E,F. In this case we observed the apparent interplay of light circular polarization and flakes chirality. Plasmon-assisted CV degradation proceeds significantly faster when the combination of RCP light and $Ti_3C_2T_x$-(P)-Hel or LCP light and $Ti_3C_2T_x$-(M)-Hel are used, compared to all other cases. Observed differences in the degradation kinetics were even more distinct than in the previous case of polarization-sensitive light to heat conversion. Despite of our expectations almost twice greater efficiency was observed for a "right" combination of flakes and light chirality. At the moment we are not able to explain so significant difference. We can only assume that the observed phenomenon is related to one (most likely non-thermal) mechanism of plasmon catalysis, which may involve either injection of hot electron in dye molecule or excitation of an internal electron in the dye molecule, both leading to molecule destabilization and degradation.[65,68] The probabilities of both processes are affected by the interplay of mutual components in chiral light–chiral catalysts–reagent system, and can have a non-trivial origin. Still unsolved problems open the avenue for further research of chiral plasmonics in triggering of organic (and other) chemical transformation.[7] To partially explain this significant difference, we performed several additional experiments aimed at revealing the CV degradation mechanism. First, we estimated the potential degradation of CV under increased temperature (based on the results of Figure 4A,B). In this case, we observed the insignificant CV degradation (Figure S11, Supporting Information). Second, according to the simple experimental route proposed in,[69] we investigated the CV degradation rate as a function of light power or illuminated area (Figure S12, Supporting Information). In these cases, we observed the close to linear and quadratic dependences respectively, which are characteristic for photochemical plasmon-assisted catalysis rather than for photothermal plasmon-assisted catalysis. Common photochemical plasmon-assisted catalysis proceeds through either the injection of a hot electron in the dye molecule or the excitation of an internal electron in the dye molecule, both leading to molecule destabilization and degradation.[65,68] To investigate the possible mechanism of plasmon catalysis further, we also performed a range of scavenging experiments, where the CV degradation was performed in the presence of $Ti_3C_2T_x$ flakes and scavengers of one of the potential reaction pathways: cyclooctatetraene (COT), a triplet states quencher; 2,2,6,6-Tetramethylpiperidin-1-yl)oxy (TEMPO), a radicals quencher[70]; isopropyl alcohol (IPA), a OH radical quencher; triethanolamine (TEAO), a hole-capturer; and *p*-benzoquinone (BQ), a O_2^- quencher[65] (Figure S13 and S14, Supporting Information). Based on results obtained, we can conclude that the CV degradation can proceeds under the attack of O_2^- (which is created through plasmon assisted hot electron transfer from $Ti_3C_2T_x$ flake to dissolved oxygen) as well as through the triplet excited-state CV* excitation (and related destabilization of dye molecule).

Finally, the liquid chromatography-mass spectrometry based determination of degradation products was performed (Figure S15, Supporting Information). The results indicate that CV degradation proceeds via several reaction pathways. The dominant contribution seems to come from the mechanism related to plasmon-assisted generation of O_2^- highly reactive species and their subsequent attacking CV molecules. The degradation products were also found to be identical to those determined in,[71–73] which were formed basically by the attack of $\cdot OH$ or O_2^- radicals on CV. However, the significant inhibition of the degradation by COT suggests the involvement of another degradation pathway that occurs via the triplet excited state CV* (Figure S16, Supporting Information and related discussion).

3. Conclusion

In this work 2D material ($Ti_3C_2T_x$ flakes) with chiral optical response at the plasmon wavelengths was designed and created. Unlike previous reports, the chirality was achieved not through specific flakes' shapes but by coupling of intrinsically non-chiral plasmon-active flakes with helical dielectric molecules (helicene enantiomers, which intrinsically show a large value of optical rotation). Plasmonic chirality was achieved by coupling of intrinsically non-chiral plasmon-active flakes with helical dielectric molecules (helicene enantiomers, which intrinsically show the huge value of optical rotation). The helicene enantiomers prepared with the amino-group at position 2, subjected to diazotation were subsequently grafted to $Ti_3C_2T_x$ surface. As a result, the chirality at wavelengths related to flakes plasmon absorption appeared, which was confirmed by the CD technique and explained by the theoretical calculation of polarization-sensitive light absorption at plasmon wavelength which is due to the helicenes grafting to MXene flakes' surface. In particular, the apparent non-zero CD signal was measured

in $Ti_3C_2T_x$-Hel suspension, indicating that chirality appears in the system of non-arranged flakes, i.e., at the level of single 2D flake. To our best knowledge, this is the first demonstration of the creation of plasmon-active 2D material with a chiral response. The created $Ti_3C_2T_x$-Hel flakes were subsequently used for polarization-sensitive light to heat conversion, where the heat generation can be controlled by light circular polarization. We also demonstrated the $Ti_3C_2T_x$-Hel flakes potential in plasmon-assisted photochemistry, where efficiency of model organic transformation was also controlled by the interplay of flakes chirality and used light circular polarization.

4. Experimental Section

Detailed description of used materials, samples preparation and characterization are given in Supporting Information. Briefly, $Ti_3C_2T_x$ flakes were prepared by etching and delaminating of previously synthesized MAX phase. 2-Amino-substituted[6] helicene enantiomers were prepared according to the modified published procedure.[74] 2-Amino[6]helicene enantiomers (further refereed as (P)-Hel and (M)-Hel) were diazotated yielding diazonium salts[75] and subsequently grafted to $Ti_3C_2T_x$ flakes surface (created materials were designated as $Ti_3C_2T_x$(P)-Hel and $Ti_3C_2T_x$-(M)-Hel, according to grafted helicene enantiomers).

Supporting Information

Supporting Information is available from the Wiley Online Library or from the author.

Acknowledgements

This work was supported by the GACR under the project 20–19353S.

Conflict of Interest

The authors declare no conflict of interest.

Data Availability Statement

The data that support the findings of this study are available from the corresponding author upon reasonable request.

Keywords

helicene, light-to-heat conversion, MXene, photocatalysis, plasmon chirality

Received: November 3, 2022
Revised: March 27, 2023
Published online: April 23, 2023

[1] J. L. Bada, *Nature* **1995**, *374*, 594.
[2] W. Ma, L. Xu, A. F. De Moura, X. Wu, H. Kuang, C. Xu, N. A. Kotov, *Chem. Rev.* **2017**, *117*, 8041.
[3] J. R. Brandt, F. Salerno, M. J. Fuchter, *Nat Rev Chem* **2017**, *1*, 0045.
[4] N. S. Shahana Nizar, M. Sujith, K. Swathi, C. Sissa, A. Painelli, K. G. Thomas, *Chem. Soc. Rev.* **2021**, *50*, 11208.
[5] X. Mu, L. Hu, Y. Cheng, Y. Fang, M. Sun, *Nanoscale* **2021**, *13*, 581.
[6] S. X. Leong, C. S. L. Koh, H. Y. F. Sim, Y. H. Lee, X. Han, G. C. Phan-Quang, X. Y. Ling, *ACS Nano* **2021**, *15*, 1817.
[7] Y. Negrín-Montecelo, A. Movsesyan, J. Gao, S. Burger, Z. M. Wang, S. Nlate, E. Pouget, R. Oda, M. Comesaña-Hermo, A. O. Govorov, M. A. Correa-Duarte, *J. Am. Chem. Soc.* **2022**, *144*, 1663.
[8] W. Wu, M. Pauly, *Adv. Mater.* **2022**, *3*, 186.
[9] G. Zheng, J. He, V. Kumar, S. Wang, I. Pastoriza-Santos, J. Pérez-Juste, L. M. Liz-Marzán, K.-Y. Wong, *Chem. Soc. Rev.* **2021**, *50*, 3738.
[10] N. H. Cho, G. H. Byun, Y.-C. Lim, S. W. Im, H. Kim, H.-E. Lee, H.-Y. Ahn, K. T. Nam, *ACS Nano* **2020**, *14*, 3595.
[11] G. González-Rubio, J. Mosquera, V. Kumar, A. Pedrazo-Tardajos, P. Llombart, D. M. Solís, I. Lobato, E. G. Noya, A. Guerrero-Martínez, J. M. Taboada, F. Obelleiro, L. G. MacDowell, S. Bals, L. M. Liz-Marzán, *Science* **2020**, *368*, 1472.
[12] W. Yan, L. Xu, C. Xu, W. Ma, H. Kuang, L. Wang, N. A. Kotov, *J. Am. Chem. Soc.* **2012**, *134*, 15114.
[13] S. Chen, Z. Liu, H. Du, C. Tang, C.-Y. Ji, B. Quan, R. Pan, L. Yang, X. Li, C. Gu, X. Zhang, Y. Yao, J. Li, N. X. Fang, J. Li, *Nat. Commun.* **2021**, *12*, 1299.
[14] N. Liu, H. Liu, S. Zhu, H. Giessen, *Nat. Photonics* **2009**, *3*, 157.
[15] M. Liu, E. Plum, H. Li, S. Li, Q. Xu, X. Zhang, C. Zhang, C. Zou, B. Jin, J. Han, W. Zhang, *Adv. Funct. Mater.* **2021**, *31*, 2010249.
[16] Y. Kalachyova, O. Guselnikova, R. Elashnikov, I. Panov, J. Žádný, V. Církva, J. Storch, J. Sykora, K. Zaruba, V. Švorčík, O. Lyutakov, *ACS Appl. Mater. Interfaces* **2019**, *11*, 1555.
[17] G. Zheng, Z. Bao, J. Pérez-Juste, R. Du, W. Liu, J. Dai, W. Zhang, L. Y. S. Lee, K.-Y. Wong, *Angew. Chem., Int. Ed.* **2018**, *57*, 16452.
[18] B. M. Maoz, Y. Chaikin, A. B. Tesler, O. Bar Elli, Z. Fan, A. O. Govorov, G. Markovich, *Nano Lett.* **2013**, *13*, 1203.
[19] X. Lan, X. Zhou, L. A. McCarthy, A. O. Govorov, Y. Liu, S. Link, *J. Am. Chem. Soc.* **2019**, *141*, 19336.
[20] A. O. Govorov, Z. Fan, P. Hernandez, J. M. Slocik, R. R. Naik, *Nano Lett.* **2010**, *10*, 1374.
[21] E. Miliutina, J. Zadny, O. Guselnikova, J. Storch, H. Walaska, A. Kushnarenko, V. Burtsev, V. Svorcik, O. Lyutakov, *Sens. Actuators, B* **2021**, *343*, 130122.
[22] D. Vestler, A. Ben-Moshe, G. Markovich, *J. Phys. Chem. C* **2019**, *123*, 5017.
[23] K. H. Park, J. Kwon, U. Jeong, J. Y. Kim, N. A. Kotov, J. Yeom, *ACS Nano* **2021**, *15*, 15229.
[24] T. Levi-Belenkova, A. O. Govorov, G. Markovich, *J. Phys. Chem. C* **2016**, *120*, 12751.
[25] F. Lu, Y. Tian, M. Liu, D. Su, H. Zhang, A. O. Govorov, O. Gang, *Nano Lett.* **2013**, *13*, 3145.
[26] L. Tian, C. Wang, H. Zhao, F. Sun, H. Dong, K. Feng, P. Wang, G. He, G. Li, *J. Am. Chem. Soc.* **2021**, *143*, 8631.
[27] L. M. Kneer, E.-M. Roller, L. V. Besteiro, R. Schreiber, A. O. Govorov, T. Liedl, *ACS Nano* **2018**, *12*, 9110.
[28] L. M. Kneer, E.-M. Roller, L. V. Besteiro, J. Kumar, F. J. García de Abajo, L. Galantini, *ACS Nano* **2020**, *14*, 16712.
[29] S. Gao, J. Liu, W. Zhang, *J. Phys. Chem. C* **2016**, *120*, 10500.
[30] N. A. Abdulrahman, Z. Fan, T. Tonooka, S. M. Kelly, N. Gadegaard, E. Hendry, M. Kadodwala, A. O. Govorov, *Nano Lett.* **2012**, *12*, 977.
[31] V. K. Valev, J. J. Baumberg, C. Sibilia, T. Verbiest, *Adv. Mater.* **2013**, *25*, 2517.
[32] J. Kumar, K. G. Thomas, L. M. Liz-Marzan, *Chem. Comm.* **2016**, *52*, 12555.
[33] A. García-Etxarri, J. A. Dionne, *Phys. Rev. B* **2013**, *87*, 235409.
[34] S. Yoo, Q. H. Park, *Sci. Rep.* **2015**, *5*, 14463.
[35] M. Naguib, M. Kurtoglu, V. Presser, J. Lu, J. Niu, M. Heon, L. Hultman, Y. Gogotsi, M. W. Barsoum, *Adv. Mater.* **2011**, *23*, 4248.
[36] Y. Dong, S. Chertopalov, K. Maleski, B. Anasori, L. Hu, S. Bhattacharya, A. M. Rao, Y. Gogotsi, V. N. Mochalin, R. Podila, *Adv. Mater.* **2018**, *30*, 1705714.

[37] A. Zabelina, D. Zabelin, E. Miliutina, J. Lancok, V. Svorcik, S. Chertopalov, O. Lyutakov, *J. Mater. Chem. A* **2021**, *9*, 17770.7.
[38] F. Purcell-Milton, R. B. McKenna, C. P. Cullen, L. Guillemeney, N. V. Tepliakov, A. S. Baimuratov, I. D. Rukhlenko, T. S. Perova, G. S. Duesberg, A. V. Baranov, A. V. Fedorov, Y. K. Gun'ko, *ACS Nano* **2018**, *12*, 954.
[39] O. Guselnikova, H. Lim, J. Na, M. Eguchi, H.-J. Kim, R. Elashnikov, P. Postnikov, V. Svorcik, O. Semyonov, E. Miliutina, O. Lyutakov, Y. Yamauchi, *Biosens. Bioelectron.* **2021**, *180*, 113109.
[40] O. Guselnikova, P. Postnikov, A. Trelin, V. Švorčík, O. Lyutakov, *ACS Sens.* **2019**, *4*, 1032.
[41] R. Tullius, A. S. Karimullah, M. Rodier, B. Fitzpatrick, N. Gadegaard, L. D. Barron, V. M. Rotello, G. Cooke, A. Lapthorn, M. Kadodwala, *J. Am. Chem. Soc.* **2015**, *137*, 8380.
[42] Z. Liu, J. Ai, P. Kumar, E. You, X. Zhou, X. Liu, Z. Tian, P. Bouř, Y. Duan, L. Han, N. A. Kotov, S. Ding, S. Che, *Angew. Chem.* **2020**, *132*, 15338.
[43] W. Li, Z. J. Coppens, L. V. Besteiro, W. Wang, A. O. Govorov, J. Valentine, *Nat. Commun.* **2015**, *6*, 8379.
[44] M. Cotrufo, C. I. Osorio, A. F. Koenderink, *ACS Nano* **2016**, *10*, 3389.
[45] A. Rafiei Miandashti, L. Khosravi Khorashad, M. E. Kordesch, A. O. Govorov, H. H. Richardson, *ACS Nano* **2020**, *14*, 4188.
[46] P. Spaeth, S. Adhikari, L. Le, T. Jollans, S. Pud, W. Albrecht, T. Bauer, M. Caldarola, L. Kuipers, M. Orrit, *Nano Lett.* **2019**, *19*, 8934.
[47] S. Shaw, J. D. White, *Chem. Rev.* **2019**, *119*, 9381.
[48] X. Wei, J. Liu, G.-J. Xia, J. Deng, P. Sun, J. J. Chruma, W. Wu, C. Yang, Y.-G. Wang, Z. Huang, *Nat. Chem.* **2020**, *12*, 551.
[49] L. K. Khorashad, L. V. Besteiro, M. A. Correa-Duarte, S. Burger, Z. M. Wang, A. O. Govorov, *J. Am. Chem. Soc.* **2020**, *142*, 4193.
[50] F. J. Garcia-Vidal, C. Ciuti, T. W. Ebbesen, *Science* **2021**, *373*, eabd0336.
[51] H. Hübener, U. De Giovannini, C. Schäfer, J. Andberger, M. Ruggenthaler, J. Faist, A. Rubio, *Nat. Mater.* **2021**, *20*, 438.
[52] Y. Zhang, L. Wang, N. Zhang, Z. Zhou, *RSC Adv.* **2018**, *8*, 19895.
[53] M. Mehdi Hasan, M. Milon Hossain, H. Kawsar Chowdhury, *J. Mater. Chem. A* **2021**, *9*, 3231.
[54] R. Li, L. Zhang, L. Shi, P. Wang, *ACS Nano* **2017**, *11*, 3752.
[55] J. D. Jackson, *Classical Electrodynamics*, 3rd ed., Wiley, New York **1998**.
[56] K. Li, T.-H. Chang, Z. Li, H. Yang, F. Fu, T. Li, J. S. Ho, P.-Y. Chen, *Adv. Energy Mater.* **2019**, *9*, 1901687.
[57] C. Korupalli, K. L. You, G. Getachew, A. S. Rasal, W. B. Direrса, M. Zakki Fahmi, J. Y. Chang, *Pharmaceutics* **2022**, *14*, 304.
[58] Y. Xia, Y. Zhou, Z. Tang, *Nanoscale* **2011**, *3*, 1374.
[59] X. T. Kong, L. Khosravi Khorashad, Z. Wang, A. O. Govorov, *Nano Lett.* **2018**, *18*, 2001.
[60] R. Li, L. Zhang, L. Shi, P. Wang, *ACS Nano* **2017**, *11*, 3752.
[61] F. Shahzad, M. Alhabeb, C. B. Hatter, B. Anasori, S. M. Hong, C. M. Koo, Y. Gogotsi, *Science* **2016**, *353*, 1137.
[62] D. Xu, Z. Li, L. Li, J. Wang, *Adv. Funct. Mater.* **2020**, *30*, 2000712.
[63] T. Yutthalekha, C. Wattanakit, V. Lapeyre, S. Nokbin, C. Warakulwit, J. Limtrakul, A. Kuhn, *Nat. Commun.* **2016**, *7*, 12678.
[64] S. Arnaboldi, M. Magni, P. R. Mussini, *Curr. Opin. Electrochem.* **2018**, *8*, 60.
[65] E. Kazuma, Y. Kim, *Angew. Chem.* **2019**, *131*, 4850.
[66] C. Boerigter, R. Campana, M. Morabito, S. Linic, *Nat. Commun.* **2016**, *7*, 10545.
[67] F. Chen, Q. Yang, C. Niu, X. Li, C. Zhang, G. Zeng, *RSC Adv.* **2015**, *5*, 63152.
[68] Z. Zhang, C. Zhang, H. Zheng, H. Xu, *Acc. Chem. Res.* **2019**, *52*, 2506.
[69] G. Baffou, I. Bordacchini, A. Baldi, R. Quidant, *Light: Sci. Appl.* **2020**, *9*, 108.
[70] O. Guselnikova, J. Váňa, L. T. Phuong, I. Panov, L. Rulíšek, A. Trelin, P. Postnikov, V. Svorcik, E. Andris, O. Lyutakov, *Chem. Sci.* **2021**, *12*, 5591.
[71] M. F. Sanakousar, V. M. Jiménez-Pérez, B. K. Jayanna, A. H. Shridhar, K. Prakash, *J Hazard Mater Adv* **2021**, *2*, 100004.
[72] Y. H. B. Liao, J. X. Wang, J. S. Lin, W. H. Chung, W. Y. Lin, C. C. Chen, *Catal. Today* **2011**, *174*, 148.
[73] C. C. Chen, H. J. Fan, C. Y. Jang, J. L. Jan, H. D. Lin, C. S. Lu, *J Photochem Photobiol A Chem* **2006**, *184*, 147.
[74] M. Jakubec, T. Beránek, P. Jakubík, J. Sýkora, J. Žádný, V. Církva, J. Storch, *J. Org. Chem.* **2018**, *83*, 3607.
[75] V. D. Filimonov, M. Trusova, P. Postnikov, E. A. Krasnokutskaya, Y. M. Lee, H. Y. Hwang, H. Kim, K.-W. Chi, *Org. Lett.* **2008**, *10*, 3961.